Published in final edited form as:
J Am Chem Soc. 2015 November 25; 137(46): 14694–14704. doi:10.1021/jacs.5b08048.

Organization and Dynamics of Receptor Proteins in a Plasma Membrane

Heidi Koldsø[*,†] and **Mark S. P. Sansom**[*]
Department of Biochemistry, University of Oxford, South Parks Road, Oxford OX1 3QU, United Kingdom

Abstract

The interactions of membrane proteins are influenced by their lipid environment, with key lipid species able to regulate membrane protein function. Advances in high resolution microscopy can reveal the organisation and dynamics of proteins and lipids within living cells at resolutions < 200 nm. Parallel advances in molecular simulations provide near-atomic resolution models of the dynamics of the organisation of membranes of *in vivo* like complexity. We explore the dynamics of proteins and lipids in crowded and complex plasma membrane models, thereby closing the length and complexity gap between computations and experiments. Our simulations provide insights into the mutual interplay between lipids and proteins in determining mesoscale (20 to 100 nm) fluctuations of the bilayer, and in enabling oligomerization and clustering of membrane proteins.

Keywords

Coarse-grained simulations; GPCR; molecular dynamics; plasma membrane; experimental length scales

Introduction

Cell membranes are crowded and spatially heterogeneous environments for proteins. Recent advances in lipidomics have provided insights into the diversity of lipids and their biological roles (1, 2). The composition of a cell membrane depends on the cell type and also on the organelle in which it is present (3). Thus the human plasma membrane (PM) is composed of glycerolipids, sphingolipids, and sterols including cholesterol (Chol) and the composition of the lipids within the plasma membrane is asymmetric between the outer and inner leaflets (2–8). The outer leaflet is composed mostly of phosphatidylcholine (PC) and sphingomyelin (Sph) along with glycosphingolipids such as monosialodihexosylganglioside (GM3), and also Chol. The inner leaflet also contains Chol, alongside phosphoethanolamine (PE), phosphoserine (PS) and phosphatidylinositols (PIs) such as phosphatidylinositol-4,5-bisphosphate (PIP_2). The presence of PS and PIs results in the inner leaflet of the plasma membrane being anionic in nature (3–5, 9). In addition to improved descriptions of their

[*]Corresponding Authors: Heidi.Koldso@DEShawResearch.com or mark.sansom@bioch.ox.ac.uk Phone: +44 (0)1865 613304.
[†]**Present Addresses**
D. E. Shaw Research, 120 W. 45th st., 39th fl., New York, NY 10036

Europe PMC Funders Author Manuscripts

compositional complexity, it is increasingly evident that cell membranes do not function simply as a barrier between cellular compartments, but are involved in regulation of membrane protein function, in membrane trafficking, and in membrane compartmentalization via formation of lipid nanodomains/rafts (3, 10–15).

Recent advances in super-resolution microscopy have resulted in a greatly improved understanding of the dynamic localization of proteins and lipids within the membranes of living cells (7, 16–19). For example, high resolution methodologies such as stimulated emission depletion (STED) microscopy have revealed the heterogeneity of organization of both lipids and proteins within cell membranes at resolutions < 200 nm (16, 17, 19–21). In parallel with developments in cell imaging, computational approaches now enable us to explore in detail the structural and dynamic properties of model membranes (22). However, computer simulation studies of membranes have only recently moved towards development of more biologically realistic membrane models (23–26). This has allowed us and others to explore, for example, the formation of lipid nanodomains within plasma membrane models (23, 25), and to explore the ability of receptors to induce local lipid clusters (24, 27).

Coarse grained (CG) molecular dynamics simulations, as exemplified by the MARTINI methodology (28–30), are capable of modelling *in vivo* membrane complexity (23, 25, 26) and also in principle of approaching experimental length scales of 100 nm and above. Here we present the first such studies that close the length and complexity gap between simulations and experiments such as superresolution microscopy. We have constructed CG models that model key aspects of compositional complexity and molecular crowding within a mammalian plasma membrane, at length scales > 100 nm and thus directly comparable with current experimental approaches. We explore the behaviour of complex asymmetric plasma membrane models with and without two types of crowded membrane proteins present. These simulations reveal lipid-mediated oligomerisation of proteins into nanoscale domains, accompanied by reduction of the diffusion rates of proteins and lipids. This indicates that complexities in lateral organization are an intrinsic and emergent property of complex and crowded cell membranes, independent of but open to modulation by interactions of membrane proteins with the underlying cytoplasmic cytoskeleton.

Methods

Setup of the PM system

The membrane model consisted of a plasma membrane-like lipid mixture, with an outer leaflet composed of PC:PE:Sph:GM3:Chol (40:10:15:10:25) and inner leaflet of PC:PE:PS:PIP_2:Chol (10:40:15:10:25). PC, PE, PS were modelled with 1-palmitoyl-2-oleoyl (PO) lipid tails (i.e. each with one unsaturated bead) while Sph and GM3 were modeled with the ceramide tail with one unsaturated bead. PIP_2 was modeled using a fully saturated tail. The plasma membrane model (PM) without any proteins consisted of 54,000 lipids, as was built from a 6,000 lipid plasma membrane model described earlier (23). The 6,000 lipid patch was constructed from a pure PC bilayer which was converted into the desired asymmetric membrane model by either renaming and thereby exchange of lipids same size or smaller than PC or alignment and substitution for larger lipids (such as GM3 and PIP_2) as described previously in Koldsø *et al.* (23). The 6,000 lipid patch was concatenated onto a

3×3 system resulting in a 54,000 lipid system with a plasma membrane-like composition. The standard MARTINI water model was used and the system was neutralised using NaCl to a 0.15 M concentration. The resultant system consisted of a total of 2.28 M particles (see also Table S1). The parameters for PC, PE, PS, Sph and cholesterol was obtained from the MARTINI webpage: (http://md.chem.rug.nl/cgmartini/images/parameters/ITP/martini_v2.0_lipids.itp), while parameterisation of GM3 and PIP_2 has been described previously (23, 31)

Setup of the TMH system

The TM domain of gp130 was modelled in PyMOL (PyMOL Molecular Graphics System, Version 1.5.0.4 Schrödinger, LLC) as previously described (23, 27) and converted into coarse-grained representation using the MARTINI2.2 (28) force field. The **TMH** system was constructed based on concatenating 6×6 of a system containing 16 gp130 TM helixes within a plasma membrane model (see above) consisting of 1,756 lipids as described previously (23). The resulting system consisted of 576 copies of the gp130 TM helix and 63,342 lipids. The standard MARTINI water model was applied and the system was neutralised using a NaCl concentration of 0.15M which yielded a total of 2.69 M particles (see also Table S1).

Setup of the GPCR receptor system

The structure of the S1P1 receptor was derived from PDBcode:3V2W (32). The T4 lysozyme insert used in the structure determination was removed and missing residues 12-16, 40-46, 149-155, 232-243, 326-330 were modelled using Modeller 9.10 (33), which yielded a protein model consisting of residues 12-330. Additionally the genome sequence (K250, S251, L252) from UNIPROT (P21453) was used instead of the NV sequence from the epithelium used by the authors of the crystal structure (32). The atomistic S1P1 receptor model was energy minimized using a steepest descent method prior to being converted into CG representation using the MARTINI2.2 force field and the ELNEDYN (34) elastic network model. A single CG model of S1P1 was embedded into a PC bilayer through a 25 ns self-assembly simulation (35). The PC membrane was subsequently converted into a plasma membrane model utilizing the in-house exchange lipid methodology (see above) to the same composition as the **PM** model. The system containing the S1P1 receptor embedded into a plasma membrane model was then equilibrated for 10 ns prior to being concatenated into a 12×12 system. The resulting system contained 144 repeats of the S1P1 receptor proteins, 59,616 lipids and was solvated with the standard MARTINI water model and neutralised to a 0.15 M NaCl concentration. The **GPCR** system thus contained 2.60 M particles (see also Table S1).

Coarse-grain molecular dynamics (CG-MD) simulations

All simulations were performed using GROMACS 4.6 (36) (www.gromacs.org) and the standard MARTINI protocol. Periodic boundary conditions were applied and a timestep of 20 fs was applied in all the simulations. The temperature was maintained at 323 K using a Berendsen thermostat (37) and the pressure at 1 bar using a Berendensen barostat. For both the temperature and pressure a coupling constant of 1 ps was used for the **PM** and **TMH**

system, while a coupling constant of 4 ps was used for the **GPCR** system. In all simulations the reaction field coulomb type was used with a switching function from 0.0 to 1.2 nm, and the van der Waals interactions were treated using a cut-off with a switching function from 0.9 to 1.2 nm. The LINCS algorithm was used to constrain covalent bonds to their equilibrium values (38). All three systems were simulated for 10 μs of production run.

Analysis

Diffusion coefficients were calculated using from the mean square displacement at various intervals using a timestep of 5 ns and and the density distribution of lipid head groups were obtained through using *g_msd* and *g_density* in gromacs respectively. VMD plugins were used to compute radial distribution functions (39, 40). Contact data was obtained from in house scripts and visualisation in VMD (40). The protein cluster analysis was based on MDAnalysis (41) and in house scripts.

Results

Three dynamic membrane systems

Three large (ca. 140 x 140 nm^2, see Table S1 for details) plasma membrane model systems were constructed (Figure 1). Each of these was based upon an asymmetric lipid bilayer. The composition of the extracellular leaflet was: PC:PE:Sph:GM3:Chol = 40:10:15:10:25, and of the intracellular leaflet was: PC:PE:PS:PIP_2:Chol = 10:40:15:10:25.

The first system was a plasma membrane (PM; Fig. 1a) lipid bilayer without any proteins present. This provided a control for comparison with two systems containing multiple copies of proteins at biologically relevant degrees of crowding. A simple protein-containing system (**TMH**; Fig. 1B), based on previous smaller scale studies (23), contained 576 copies of a single α-helical transmembrane (TM) domain (that of the gp130 cytokine receptor) including short (4 residue) juxtamembrane domains on each side of the membrane. In this system the protein occupied approximately 6% of the cross-sectional area of the membrane. A more complex model (**GPCR**; Fig. 1c) was constructed from a large PM patch into which 144 copies of a GPCR were inserted, the proteins thus occupying 12% of the area of the membrane. This enabled us to probe the nanoscale organization and dynamics of a pharmaceutically important GPCR (the sphingosine-1-phosphate 1 receptor (32) PDB: 3V2W). The S1P1 receptor is a target for the lipid-like drug fingolimod which is used to treat multiple sclerosis (42).

Each of the three membrane systems was simulated for 10 μs. Substantial differences in the dynamic behaviour of the membranes were observed based on the presence or absence of membrane proteins and on the nature a degree of crowding of the protein incorporated (Figure 1 and 2; SI movies S1–3). In particular, it is evident that the degree of local curvature and membrane dynamics is strongly dependent on the nature of the simulation system. Within the **PM** model without proteins we observed large scale membrane curvature/deformation (Fig. 1a and SI Fig. S1). This degree of local membrane deformation is suggestive of incipient budding and/or tubulation of the (asymmetric) membrane, but as neither proteins nor an underlying cytoskeleton is present, it may be more representative of

in vitro than of *in vivo* behaviour of cell membranes. Examination of the **TMH** and **GPCR** simulations indicates that the presence of (crowded) membrane proteins stabilised the fluctuation and curvature of the membrane, with a greater degree of stabilization of planarity correlating with an increased degree of crowding, such that the bilayer fluctuates less in the **GPCR** system (ca. 12% protein) than in the **TMH** system (ca. 6% protein).

Membrane Area per lipid

All simulations started from a planar membrane model. To ensure that the area per lipid is the same in both leaflets of the asymmetric bilayers we tested the area per lipid for the different lipid species as described previously (23). We have now extended this analysis, using APL@Voroni (43) to evaluate area per lipid for each of the different lipid species in the different bilayers. This analysis (summarized in the Supporting Information, Table S2 and Figures S2 to S7) shows that the area per lipid overall and that for each lipid species are the same for both symmetric and asymmetric membrane simulations. (Each condition was tested using simulations of small bilayers of 1500 lipids with the same lipid composition as the large PM system). Hence we are confident that the dynamics and curvature of the membranes during simulations do not arise from differences in area per lipid between the two leaflets of the PM and derived models.

Additionally we calculated the average area per lipid of each lipid species within the **PM**, **TMH** and **GPCR** systems over the initial period (1 to 3 μs) of the three simulations (Table S3). Overall we see the same average areas per lipid for each lipid species when compared to a smaller protein free plasma membrane model (Table S2 and Fig S6, S7). The largest difference observed is for PIP_2 which has a lower area within the **GPCR** system, which is most likely a result of local tight clustering of this lipid around the protein when the GPCR is present (see below).

Membrane fluctuations and deformations

Significant fluctuations were observed within the first few microseconds and continued throughout the simulation (Figure 2). Comparable fluctuations have been seen in smaller (6,000 lipid) PM models (23), and in a number of extended simulations of simple lipids bilayers (44). The visualization in figure 2 suggests that the overall amplitude of the fluctuations is dependent on the simulation systems such that **PM** > **TMH** > **GPCR**. This was quantified via normalised density distribution of the lipid head groups averaged over the course of the simulations (Figure 3). This analysis confirms that the protein free **PM** system showed the largest fluctuations and deformations of the planar bilayer, these fluctuations becoming most pronounced over the second half of the simulation. This suggests that the large membrane deformation is not a result of the initial setup of the system, as relatively stable fluctuations are observed in the first part of the simulation before a large deformation spontaneously occurs (Figure 2 and 3a)

Similarly the large curvature observed for the **TMH** system (Figure 1 and 2) is reflected in the head group density distribution (Figure 3b).

As seen for the protein free system, large (> 40 nm) scale fluctuations are observed throughout the **TMH** simulation, starting within the first 0.5 μs and reaching their largest extent over the final 4 μs. The curvature in the **TMH** system is less localized than in the **PM** system without any proteins, as indicated by comparison of the shapes of the 8-10 μs distributions for the two systems (Figure 1-3). Significantly, the more crowded (12% protein fractional area) **GPCR** system showed much smaller membrane fluctuations than observed for the other two simulations. This can be seen from the head-group distribution, which reveals a bimodal structure typical of a planar bilayer projected onto the normal (i.e. z-axis) for the first half of the simulation (Figure 3c).

We further analysed the extent of the membrane deformation by examining the final (10 μs) system configurations according to the z-positions of the lipid head groups (Figure 4). This reveals that the **PM** system without proteins has a clear localized deformation, ~20 nm in diameter and extending at its peak beyond 25 nm on z. A substantive (25 nm on z) deformation is also observed for the **TMH** system, but for this system (containing ca. 6% protein) the curvature is less localised and more evenly distributed throughout the system. In contrast, for the **GPCR** system the curvature is much less localized within the plane of the bilayer and as noted above is of significantly smaller amplitude.

From this combination of analyses, it is clear that the presence of a complex membrane protein in a crowded system stabilizes the (mixed lipid and asymmetric) bilayer against large amplitude fluctuations on a microsecond timescale. In principle, analysis of these fluctuations in the context of Helfrich-Canham (HC) elastic theory may be used to derive a membrane bending modulus. However, HC analysis is not strictly applicable to asymmetric membranes and so has not been applied in the current study.

Since both the transmembrane helix and the GPCR are more or less cylindrical in cross section, the ‘damping’ effect is more likely to be a result of crowding rather than the protein shape. However the role of the shape of transmembrane domains (e.g. some potassium channels are conical in shape) in modulating dynamic fluctuations of membranes will be of interest to explore further.

Lipid diffusion

To explore the local dynamics of the different lipid species and the proteins we calculated the diffusion coefficient of the different lipids species throughout the simulations. A number of studies on simpler membrane systems, both experimental (45, 46) and computational (47–50) have indicated that crowding may slow lateral diffusion of both lipids and proteins. Diffusion coefficients were derived from mean square displacement measurements of lipids and of proteins. Within the **PM** system (i.e. without any proteins present, Fig. 5) we observed slower diffusion of GM3 relative to other lipids, as previously seen in smaller membrane simulations (23), and as has been observed for glycolipids in living cells (16). The presence of crowded single TM helices (**TMH**; Fig. 5) did not change the overall pattern of diffusion of the lipids. As anticipated the protein diffused more slowly than the lipids. However, a significant difference was observed in the presence of the GPCRs (**GPCR**; Fig. 5). Overall, the crowding effect of this protein reduced lipid diffusion coefficients by a factor of ca. 1.5. This in turn suggests that the observed decrease in bilayer

undulations in the presence of GPCRs is not simply a consequence of slower lipid diffusion, as the GPCR undulations after 10 μs are smaller than the PM undulations after 2 μs. This slowing of lipid diffusion was especially clear for cholesterol and for PIP_2. Not surprisingly given the difference in protein size, the diffusion of the S1P1 receptor is slower than was observed for the single TM domain of gp130. Overall, our calculations of lipid diffusion coefficients indicate that protein crowding slows lipid diffusion in a similar manner to that seen previously from experiments and simulations, and that this effect is more marked for those lipids (e.g. cholesterol, PIP_2) which interact specifically with membrane proteins. This latter observation suggests that slower lipid diffusion is because the more tightly interacting lipids diffuse together with the proteins with which they interact.

Protein-lipid interactions

A global picture of protein-lipid interactions may be obtained from evaluation of radial distribution function of lipids around the proteins within the two systems containing proteins (Figure 6 and S8). This analysis revealed comparable behaviour between the two different protein systems, with the main protein-lipid interactions being with PIP_2, with cholesterol (Figure 6), and with GM3 (Figure S8). We have explored the protein-lipid interactions pattern of these three selected lipids in more detail by calculating the mean frequency of interaction between the lipid species and the different residues of each protein averaged over the entire simulation. For the **TMH** simulation we observed the pattern of behaviour described previously for smaller and shorter simulations. In particular PIP_2 was observed to form specific interactions with the C-terminal juxtamembrane basic residues (23), as has also been observed in simulations of receptor tyrosine kinase TM+JM domains in (simple) lipid bilayers17. For the **GPCR** system we observed clear patterns of interactions of PIP_2 and of cholesterol with the S1P1 receptor protein (Figure 7).

The intracellular facing surface of the S1P1 receptor is enriched in basic residues (as is frequently the case for transmembrane proteins (6, 24)). These basic residues form frequent interactions with the headgroup of PIP_2 molecules within the intracellular leaflet of the membrane, explaining the reduced mobility of PIP_2 when S1P1 receptors are present (see Figure 5). Given the interactions between PIP_2 and the S1P1 receptors are evenly distributed around the intracellular face of the protein, the anionic lipid seems to form an annulus around the protein (51–54). This annular interaction between PIP_2 and S1P1 receptors is found in all 144 proteins for over 75 % of the simulation time, indicating that this lipid indeed forms a stable layer around the protein.

The interactions of GPCRs and cholesterol are of especial interest as it has been suggested that cholesterol is able to regulate GPCR function (13). Cholesterol has been found to stabilise the dimerization interface of class C GPCRs (55), and bound cholesterol molecules are seen in the crystal structures of a number of class A GPCRs (56, 57) (although not the S1P1). We observed that hydrophobic residues on lipid-exposed surfaces of each of the TM helices of the S1P1 formed interactions with cholesterol over the entire simulation time in all 144 S1P1 receptors, and annulus of cholesterol around the GPCR (Fig. 7b). Furthermore, residues on the extracellular surfaces of TM1, TM2 and TM3 formed strong interactions to the cholesterol headgroup (SI. Fig. S9). Interestingly, TM1, TM2, TM3 (in addition to TM4)

have been suggested to play a role in cholesterol mediated dimerization of metabotropic glutamate receptor (55) and in the cholesterol binding site within β2-adrenergic receptors (56–58) based on crystal structures. Additionally we observe a clear cholesterol headgroup interaction site involving two basic residues within the intracellular segments of TM5 and TM6 (SI. Fig. S9). This is of potential interest, especially as TM6 movement is believed to be involved in the main conformations change upon activation of GPCRs (59).

The interaction between PIP_2 and protein was stable and specific, with the lipid remaining largely bound throughout the simulation for each copy of the protein (Fig. S10). In contrast, cholesterol interacts more transient: cholesterol was observed to bind and dissociate throughout the simulations on a sub-microsecond timescale (Fig. S11).

Protein oligomerization

Visualization of the **TMH** simulation (Fig. 4b and SI movie S2) reveals oligomerization of the gp130 TM helices. In previous smaller scale simulations formation of TM dimers and trimers was observed (23). Thus, the current large scale simulations allow us to explore in more detail clustering/oligomerization of both simple (**TMH**) and more complex (**GPCR**) membrane proteins. Examination of the GPCR simulation (Fig. 4cd and SI movie S3) suggests that whilst for most of the time the S1P1 receptors are largely present as monomers, transient dimers can be seen and occasionally trimeric and larger scale clusters appear. This may be compared to e.g. previous CG studies of rhodopsin (up to 64 proteins in a simulation) within simple model membranes which revealed formation of linear assemblies of the GPCR (60, 61). In our simulations rather than large assembles of GPCRs we observe that the S1P1 receptor monomers come into proximity to each other, sometimes form small oligomers (dimers, trimers, etc.) which subsequently dissociate allowing monomers to diffuse away from each other (SI Movie S3). This association and dissociation of the S1P1 receptor monomers during the simulation suggests a more dynamic behaviour of protein-protein interactions of GPCRs may be seen when they are simulated within '*in vivo*' like bilayers compared to simpler membranes previously use computationally.

One may quantify the formation of dimers and higher oligomers during the **TMH** and **GPCR** simulations. For the **TMH** simulation within the first microsecond of the simulation more than 50% of the **TM** helices form dimers and higher oligomers, and after approximately 5 μs of simulation the oligomerization pattern appears to have reached a plateau (SI Fig. S12) such that the system is a mixture of dimers, trimers and higher order oligomers in addition to a small (20% or less) fraction of monomers. Significantly, the proteins do not assemble into one large cluster, but rather exist as a mixture of smaller localized oligomers (Figure 4b). In contrast, for the GPCR simulation (Figure 8a) there is a small and slow decline in the fraction of monomeric proteins, such that in the latter part of the simulation the systems consists of largely monomers with a small fraction of dimers (~20%) and trimers (~5%).

As discussed above, lipids form co-clusters with the proteins in both the **TMH** and the **GPCR** systems and in particular cholesterol, PIP_2 and GM3. A number of studies have suggested that lipid mediated effects may influence protein-protein interactions within membranes (60, 62–65). Detailed examination of S1P1 dimers observed in the **GPCR**

simulation suggests that indeed cholesterol may mediate the protein-protein interactions (Fig. 8b-d). Taken together, these results indicate that co-clustering of proteins and lipids strongly influences the dynamics and organisation of the S1P1 receptor within the (model) plasma membrane.

Discussion

The simulations presented here allow us for the first time to explore the dynamics of protein and lipids at experimental length scales in an *in vivo* like environment. The presence of large numbers of copies of membrane proteins in our simulations allows us to gather statistically significant information on protein and lipid diffusion and on protein-lipid interactions in membranes where the degree of crowding approaches that seen in cell membranes (66). Our simulations of complex asymmetric membranes with and without membrane proteins are at length scales comparable to those accessible by experiments such as STED (16) microscopy, and the degree of complexity approaches that found in plasma membranes (2–4, 8–10, 67). These models therefore provide a valuable complement to aid interpretation of experimental data. For example, we may compare the large fluctuations in our **PM** simulations with the experimentally observed formation of blebs in regions of plasma membrane which are separated from the underlying cytoskeletal cortex (68). Such blebs are micron-sized, and so the sub-micron scale of the large deformations observed in our simulations (performed in the absence of any model of the cytoskeletal cortex) may correlate with the early events of bleb formation.

We are able to observe differences in membrane dynamical fluctuations and in lipid diffusion depending on the system studied. In particular, the membrane proteins have a significant effect on the fluctuations and undulations of the plasma membrane. We have observed restricted movement of particular the glycolipid GM3 and of PIP_2, similar to what has been observed in smaller simulation systems (23, 25). This is in agreement with experimental observations showing anomalous diffusion of another glycolipid, GM1, in living cells (16, 69). Importantly, we see that the extent and the dynamics of protein clustering and oligomerization depend on the nature of the membrane protein embedded within the plasma membrane model. Thus, as a single TM helix from the cytokine receptor gp130 clusters rapidly into oligomers, whilst a G-protein coupled receptor (S1P1) seems to form ‘looser’ oligomers in which the protein-protein interactions are mediated by lipids, especially cholesterol.

We have previously explored the effect of protein crowding on lipid mobility and complexity on smaller length scales (23, 47). Here we move closer towards simulations of biologically realistic membranes at experimentally relevant length scales. Our models still, of course, are an approximation to the membranes of living cells. In particular, we note the absence of a model of the underlying cytoskeleton from our simulations. However, since membrane compartments are believed to be in the order of 40-300 nm in size, only a small number of compartments would be present within our simulation systems and this effect is believed to minimal (70). Additionally, our models only contain one single protein species, which is obviously an approximation to the multiple protein species of cell membranes. The degree of crowding effect in our models is also little lower (~6-12% membrane area occupied by

protein) compared to cell membranes which can be up to 50 % protein by mass yielding a membrane area fraction of 25 % (66) occupied by protein.

Nevertheless, these membrane models provide multiple advances compared to studies of membrane and lipid organisation in smaller systems with simple membrane compositions. We are able to observe much more dynamic organisation and oligomerization of GPCRs, which have previously been observed to form string-like oligomers when simulated in single lipid species (PC) bilayers (60, 61). We are able to explore specific-protein lipid interactions mediating the organisation of this particular GPCR, the S1P1 receptor, within the plasma membrane model. This illustrates the importance of lipid complexity in global organization of proteins within a cell membrane. For the S1P1 receptor we can identify specific interaction sites, particularly for PIP_2 molecules within the intracellular leaflet. This may allow this signalling lipid to cocluster with the S1P1 receptor, potentially modulating downstream signalling. Additionally, it has been shown that cholesterol is able to regulate the function of GPCRs (13) and interestingly we observe a strong interaction pattern between the S1P1 receptor and cholesterol within our simulations. We observe specific interactions sites of the cholesterol headgroup around residues within TM1, TM2 and TM3. These particular helices have previously been shown to form cholesterol binding sites in crystal structures of both class A (56–58) and class C (55) GPCRs. In addition we also see specific interactions between cholesterol and intracellular basic residues within TM5 and TM6. This is an interesting observation, as TM6 is particularly believed to play a key role in the activation mechanism of GPCRs as this transmembrane helix undergoes the largest conformation changes upon interactions with the associated G-protein (59). Furthermore, we also observe that cholesterol forms an annulus around the entire membrane embedded portion of the receptor.

A possible limitation of the current study is the approximations implicit in the use of coarse-grained force field. Although this approach captures many aspects of lipid-protein (71) and protein-protein interactions (60) within membranes, it has a number of limitations including the use of an elastic network model which prevents the proteins from undergoing large conformational changes, which in turn may influence their interactions. We also note that polarizable models are available for water and proteins within the MARTINI force field. However, since the lipids are currently not included in this polarizable model we have imposed a consistent level of granularity throughout the systems by using the standard (i.e. non-polarizable) MARTINI force field.

A limitation of most current simulations – even those employing coarse-grained and related methods – is that the time scales which are achievable during simulations are so short that complex systems are unlikely to reach an equilibrium or a steady state. In the current study we can see that although the simulations are approaching a steady state, it is difficult to judge whether the more complex and crowded systems are equilibrated. Future increases in computer power will help to address this limitation.

In summary, we have for the first time closed the gap between experiments and simulations both in terms of complexity and length scale at a resolution that preserves the key interactions of both the protein and lipids. The simulations presented here clearly show an

Europe PMC Funders Author Manuscripts

agreement between dynamical behaviour of lipids in living cells as illustrated by experiments (72) and the reduced mobility we observe for e.g. GM3. Additionally, these models allow us to explore the dynamical behaviour of co-clustering of proteins and lipid nanodomains. Our results illustrate that the organisation of a cell membrane is controlled by various factors, and that the protein-lipid interactions play a key role in organization within the plasma membrane. The models and methods presented here provide a generalizable computational approach to explore membrane proteins in more native-like lipid environments and thereby obtain an improved understanding of the local organisation within the cell membranes.

Supplementary Material

Refer to Web version on PubMed Central for supplementary material.

Acknowledgment

Dr. Anna Duncan is acknowledged for fruitful discussions. Dr. Tom Dunton and Dr. Joseph Goose are acknowledged for the protein cluster tool. Anna Muszkiewicz is acknowledged for initial S1P1/cholesterol simulations. Research in MSPS's group is funded by grants from the BBSRC, EPSRC, and the Wellcome Trust. HK acknowledges the Alfred Benzon foundation and the Wellcome Trust. PRACE is acknowledged for computer time.

Abbreviations

CG	Coarse grained
GPCR	G-protein coupled receptor
S1P1	sphingosine 1-phosphate receptor 1
MD	Molecular dynamics
STED	Stimulated emission depletion
Sph	Sphingomyelin
GM3	monosialodihexosylganglioside
PM	Plasma membrane
PC	phosphatidylcholine
PE	phosphatidylethanolamine
PS	phosphoserine
PIP_2	phosphatidylinositol-4,5-bisphosphate
Chol	Cholesterol
TM	transmembrane
JM	juxtamembrane

References

1. Wenk MR. Cell. 2010; 143:888–895. [PubMed: 21145456]
2. Shevchenko A, Simons K. Nat Rev Mol Cell Biol. 2010; 11:593–598. [PubMed: 20606693]
3. van Meer G, Voelker DR, Feigenson GW. Nat Rev Mol Cell Biol. 2008; 9:112–124. [PubMed: 18216768]
4. van Meer G, de Kroon AIPM. J Cell Sci. 2011; 124:5–8. [PubMed: 21172818]
5. Zachowski A. Biochem J. 1993; 294:1–14. [PubMed: 8363559]
6. Sharpe HJ, Stevens TJ, Munro S. Cell. 2010; 142:158–169. [PubMed: 20603021]
7. Spira F, Mueller NS, Beck G, von Olshausen P, Beig J, Wedlich-Soldner R. Nat Cell Biol. 2012; 14:640–648. [PubMed: 22544065]
8. Sampaio JL, Gerl MJ, Klose C, Ejsing CS, Beug H, Simons K, Shevchenko A. Proc Natl Acad Sci U S A. 2011; 108:1903–1907. [PubMed: 21245337]
9. Coskun Ü, Simons K. Structure. 2011; 19:1543–1548. [PubMed: 22078554]
10. Lingwood D, Kaiser H, Levental I, Simons K. Bio-chem Soc Trans. 2009; 37:955–960.
11. Rajendran L, Simons KJ. Cell Sci. 2005; 118:1099–1102.
12. Helms JB, Zurzolo C. Traffic. 2004; 5:247–254. [PubMed: 15030566]
13. Zocher M, Zhang C, Rasmussen SGF, Kobilka BK, Müller DJ. Proc Natl Acad Sci U S A. 2012; 109:E3463–E3472. [PubMed: 23151510]
14. Coskun Ü, Grzybek M, Drechsel D, Simons K. Proc Natl Acad Sci U S A. 2011; 108:9044–9048. [PubMed: 21571640]
15. Michailidis IE, Rusinova R, Georgakopoulos A, Chen Y, Iyengar R, Robakis NK, Logothetis DE, Baki L. Pflugers Arch - Eur J Physiol. 2011; 461:387–397. [PubMed: 21107857]
16. Eggeling C, Ringemann C, Medda R, Schwarzmann G, Sandhoff K, Polyakova S, Belov VN, Hein B, von Middendorff C, Schonle A, Hell SW. Nature. 2009; 457:1159–1162. [PubMed: 19098897]
17. Honigmann A, Mueller V, Ta H, Schoenle A, Sezgin E, Hell SW, Eggeling C. Nat Commun. 2014; 5:5412. [PubMed: 25410140]
18. Chmyrov A, Keller J, Grotjohann T, Ratz M, d'Este E, Jakobs S, Eggeling C, Hell SW. Nat Meth. 2013; 10:737–740.
19. Hosy E, Butler C, Sibarita J. Curr Opin Chem Biol. 2014; 20:120–126. [PubMed: 24975376]
20. Sahl SJ, Leutenegger M, Hell SW, Eggeling C. ChemPhysChem. 2014; 15:771–783. [PubMed: 24596277]
21. Saka SK, Honigmann A, Eggeling C, Hell SW, Lang T, Rizzoli SO. Nat Commun. 2014; 5:4509. [PubMed: 25060237]
22. Baoukina S, Mendez-Villuendas E, Bennett WFD, Tieleman DP. Faraday Discuss. 2013; 161:63–75. [PubMed: 23805738]
23. Koldsø H, Shorthouse D, Hélie J, Sansom MSP. PLoS Comp Biol. 2014; 10:e1003911.
24. Hedger G, Sansom MSP, Koldsø H. Sci Rep. 2015; 5:9198. [PubMed: 25779975]
25. Ingólfsson HI, Melo MN, van Eerden FJ, Arnarez C, Lopez CA, Wassenaar TA, Periole X, de Vries AH, Tieleman DP, Marrink SJ. J Am Chem Soc. 2014; 136:14554–14559. [PubMed: 25229711]
26. van Eerden FJ, de Jong DH, de Vries AH, Wasse-naar TA, Marrink SJ. Biochim Biophys Acta. 2015; 1848:1319–1330. [PubMed: 25749153]
27. Koldsø H, Sansom MSP. J Phys Chem Lett. 2012; 3:3498–3502. [PubMed: 26290979]
28. de Jong DH, Singh G, Bennett WFD, Arnarez C, Wassenaar TA, Schäfer LV, Periole X, Tieleman DP, Marrink SJ. J Chem Theory Comput. 2013; 9:687–697. [PubMed: 26589065]
29. Monticelli L, Kandasamy SK, Periole X, Larson RG, Tieleman DP, Marrink S. J Chem Theory Comput. 2008; 4:819–834. [PubMed: 26621095]
30. Marrink SJ, Risselada HJ, Yefimov S, Tieleman DP, de Vries AH. J Phys Chem B. 2007; 111:7812–7824. [PubMed: 17569554]
31. Stansfeld PJ, Hopkinson R, Ashcroft FM, Sansom MSP. Biochemistry. 2009; 48:10926–10933. [PubMed: 19839652]

32. Hanson MA, Roth CB, Jo E, Griffith MT, Scott FL, Reinhart G, Desale H, Clemons B, Cahalan SM, Schuerer SC, Sanna MG, et al. Science. 2012; 335:851–855. [PubMed: 22344443]
33. Sali A, Blundell TL. J Mol Biol. 1993; 234:779–815. [PubMed: 8254673]
34. Periole X, Cavalli M, Marrink S, Ceruso MA. J Chem Theory Comput. 2009; 5:2531–2543. [PubMed: 26616630]
35. Scott KA, Bond PJ, Ivetac A, Chetwynd AP, Khalid S, Sansom MSP. Structure. 2008; 16:621–630. [PubMed: 18400182]
36. Hess B, Kutzner C, van dS, Lindahl E. J Chem Theory Comput. 2008; 4:435–447. [PubMed: 26620784]
37. Berendsen HJC, Postma JPM, van Gunsteren WF, DiNola A, Haak JR. J Chem Phys. 1984; 81:3684–3690.
38. Hess B. J Chem Theory Comput. 2008; 4:116–122. [PubMed: 26619985]
39. Levine BG, Stone JE, Kohlmeyer A. J Comput Phys. 2011; 230:3556–3569. [PubMed: 21547007]
40. Humphrey W, Dalke A, Schulten K. J Mol Graph. 1996; 14:33–38. [PubMed: 8744570]
41. Michaud-Agrawal N, Denning EJ, Woolf TB, Beckstein O. J Comput Chem. 2011; 32:2319–2327. [PubMed: 21500218]
42. Rosen H, Stevens RC, Hanson M, Roberts E, Oldstone MBA. Annu Rev Biochem. 2013; 82:637–662. [PubMed: 23527695]
43. Lukat G, Krüger J, Sommer B. J Chem Inf Model. 2013; 53:2908–2925. [PubMed: 24175728]
44. Lindahl E, Edholm O. Biophys J. 2000; 79:426–433. [PubMed: 10866968]
45. Ramadurai S, Holt A, Krasnikov V, van dB, Killian JA, Poolman B. J Am Chem Soc. 2009; 131:12650–12656. [PubMed: 19673517]
46. Dix JA, Verkman AS. Annu Rev Biophys. 2008; 37:247–263. [PubMed: 18573081]
47. Goose JE, Sansom MSP. PLoS Comput Biol. 2013; 9:e1003033. [PubMed: 23592975]
48. Javanainen M, Hammaren H, Monticelli L, Jeon J, Miettinen MS, Martinez-Seara H, Metzler R, Vattulainen I. Faraday Discuss. 2013; 161:397–417. [PubMed: 23805752]
49. Domański J, Marrink SJ, Schäfer LV. Biochim Biophys Acta. 2012; 1818:984–994. [PubMed: 21884678]
50. McGuffee SR, Elcock AH. PLoS Comput Biol. 2010; 6:e1000694. [PubMed: 20221255]
51. Lee AG. Biochem Soc Trans. 2011; 39:761–766. [PubMed: 21599646]
52. Lee AG. Trends Biochem Sci. 2011; 36:493–500. [PubMed: 21855348]
53. Marsh D. Biochim Biophys Acta. 2008; 1778:1545–1575. [PubMed: 18294954]
54. Marsh D, Páli T. Biochim Biophys Acta. 2004; 1666:118–141. [PubMed: 15519312]
55. Wu H, Wang C, Gregory KJ, Han GW, Cho HP, Xia Y, Niswender CM, Katritch V, Meiler J, Cherezov V, Conn PJ, et al. Science. 2014; 344:58–64. [PubMed: 24603153]
56. Oates J, Watts A. Curr Opin Struct Biol. 2011; 21:802–807. [PubMed: 22036833]
57. Hanson MA, Cherezov V, Griffith MT, Roth CB, Jaakola V, Chien EYT, Velasquez J, Kuhn P, Stevens RC. Structure. 2008; 16:897–905. [PubMed: 18547522]
58. Stangl M, Schneider D. Biochim Biophys Acta. 2015; 1848:1886–1896. [PubMed: 25791349]
59. Rasmussen SGF, DeVree BT, Zou Y, Kruse AC, Chung KY, Kobilka TS, Thian FS, Chae PS, Pardon E, Calinski D, Mathiesen JM, et al. Nature. 2011; 477:549–555. [PubMed: 21772288]
60. Periole X, Knepp AM, Sakmar TP, Marrink SJ, Huber T. J Am Chem Soc. 2012; 134:10959–10965. [PubMed: 22679925]
61. Periole X, Huber T, Marrink S, Sakmar TP. J Am Chem Soc. 2007; 129:10126–10132. [PubMed: 17658882]
62. Parton DL, Klingelhoefer JW, Sansom MS. Biophys J. 2011; 101:691–699. [PubMed: 21806937]
63. Dunton TA, Goose JE, Gavaghan DJ, Sansom MS, Osborne JM. PLoS Comput Biol. 2014; 10:e1003417. [PubMed: 24415929]
64. de Meyer FJ, Rodgers JM, Willems TF, Smit B. Biophys J. 2010; 99:3629–3638. [PubMed: 21112287]
65. de Meyer FJ, Venturoli M, Smit B. Biophys J. 2008; 95:1851–1865. [PubMed: 18487292]

66. Dupuy AD, Engelman DM. Proc Natl Aca Sci USA. 2008; 105:2848–2852.
67. Lingwood D, Simons K. Science. 2010; 327:46–50. [PubMed: 20044567]
68. Yanase Y, Carvou N, Frohman MA, Cockcroft S. Biochem J. 2010; 425:179–193.
69. Mueller V, Ringemann C, Honigmann A, Schwarzmann G, Medda R, Leutenegger M, Polyakova S, Belov VN, Hell SW, Eggeling C. Biophys J. 2011; 101:1651–1660. [PubMed: 21961591]
70. Kusumi A, Suzuki KGN, Kasai RS, Ritchie K, Fujiwara TK. Trends Biochem Sci. 2011; 36:604–615. [PubMed: 21917465]
71. Stansfeld P, Jefferys E, Sansom MP. Structure. 2013; 21:810–819. [PubMed: 23602661]
72. Spillane KM, Ortega-Arroyo J, de Wit G, Eggeling C, Ewers H, Wallace MI, Kukura P. Nano Lett. 2014; 14:5390–5397. [PubMed: 25133992]

Europe PMC Funders Author Manuscripts

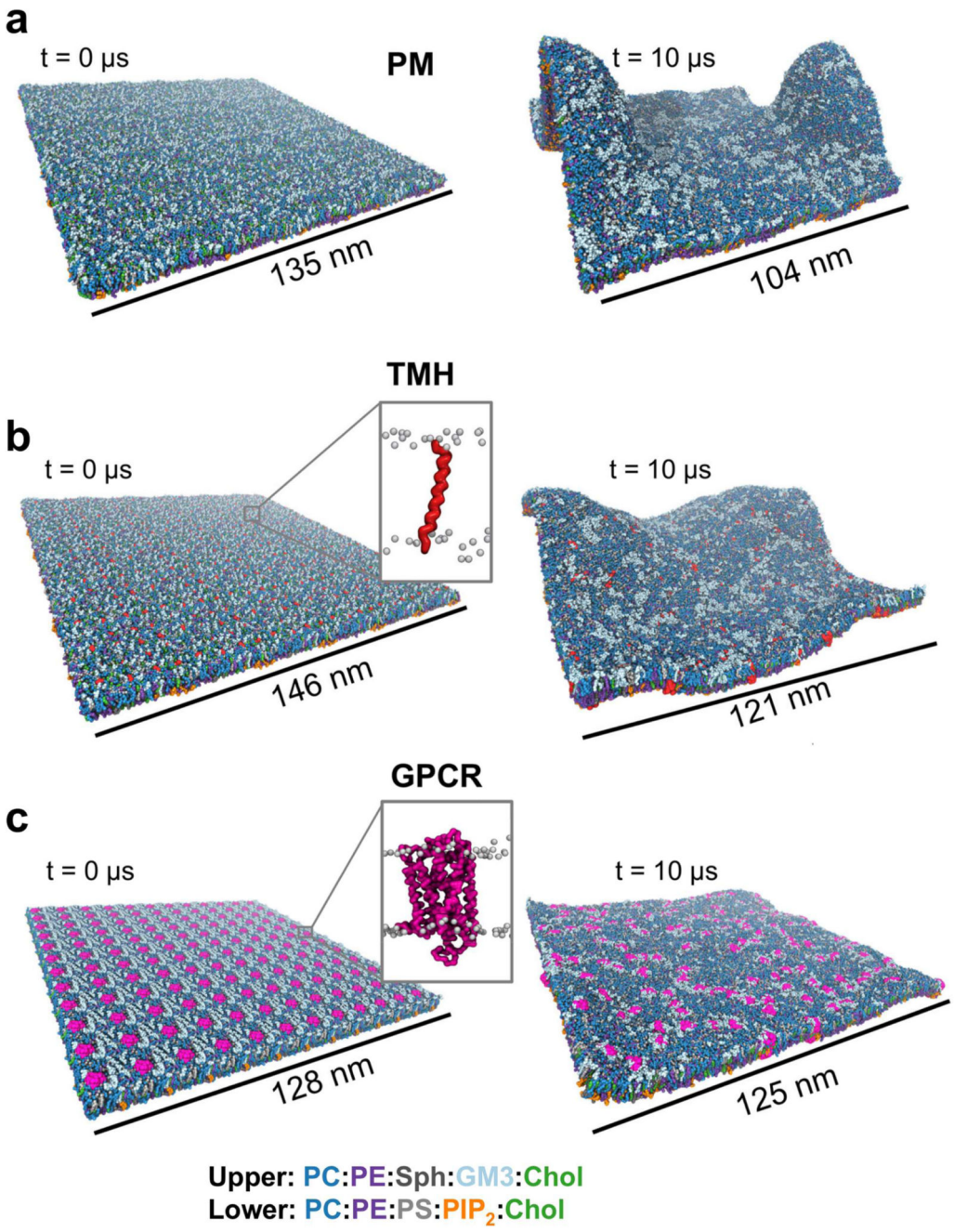

Figure 1. Membrane models at the start and end of the 10 μs simulations.

PC is shown in dark blue, PE in purple, Sphingomyelin (Sph) in dark grey, GM3 in light blue, Cholesterol (Chol) in green, PS in light grey and PIP_2 in orange. (**a**) **PM** model without any proteins consisting of 54,000 lipids; (**b**) **TMH** system containing 576 repeats of a single TM helix (in red) from the gp130 cytokine receptor and 63,342 lipids; (**c**) **GPCR** system containing 144 repeats of the S1P1 receptor (in pink) and 59,616 lipids.

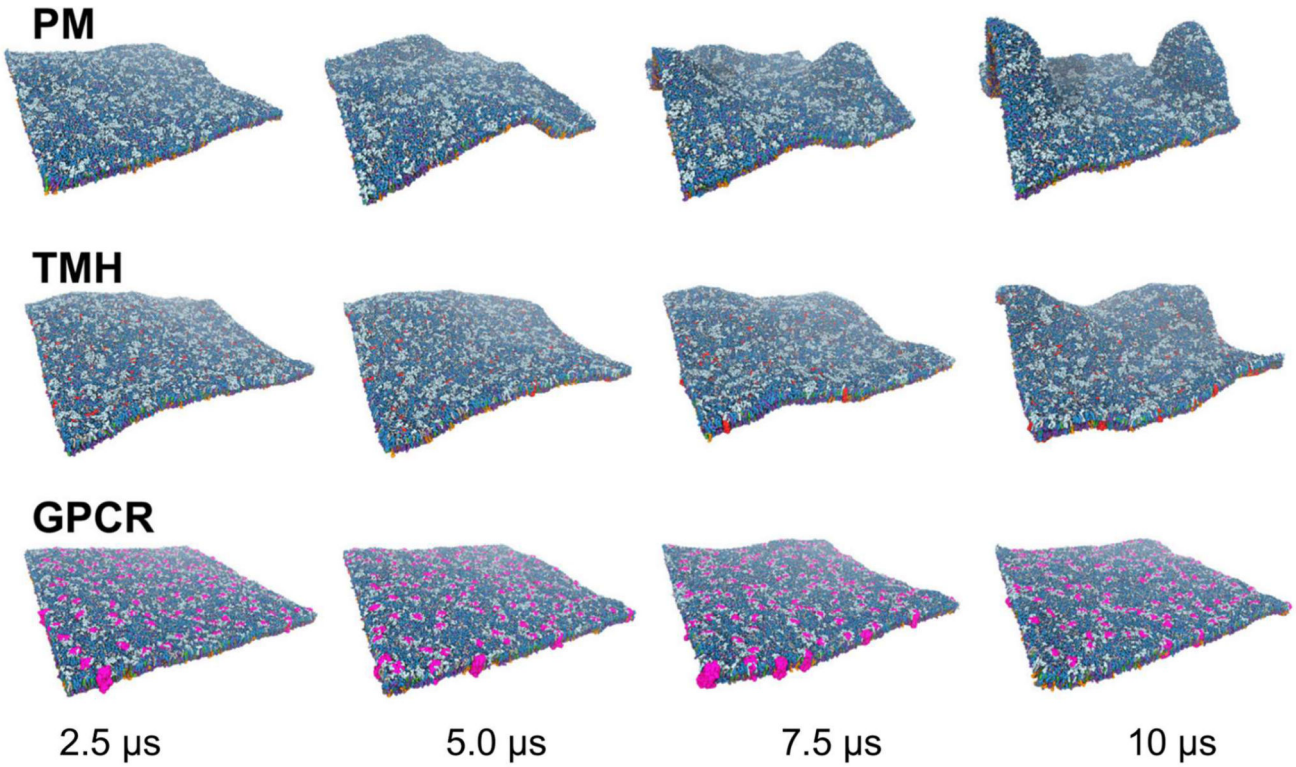

Figure 2. Dynamic evolution of membrane models.

Evolution of membrane fluctuations over time illustrated with snapshots at 2.5, 5.0, 7.5, and 10 μs of simulations for the **PM**, **TMH** and **GPCR** systems. Colours are as in Fig. 1.

Europe PMC Funders Author Manuscripts

Europe PMC Funders Author Manuscripts

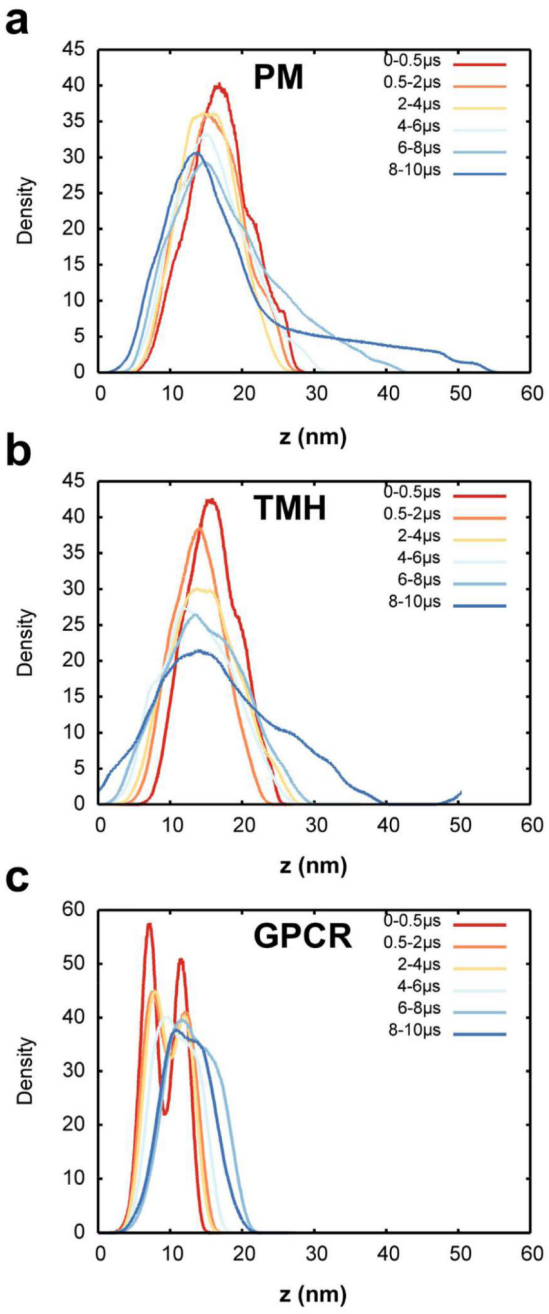

Figure 3. Lipid head group density distributions.

(**a**) Density of the head groups of all lipids except cholesterol at various intervals from the **PM** simulation. (**b**) Density of the head groups of all lipids except cholesterol at various intervals from the **TMH** simulation. (**c**) Density of the head groups of all lipids except cholesterol at various from of the **GPCR** simulation.

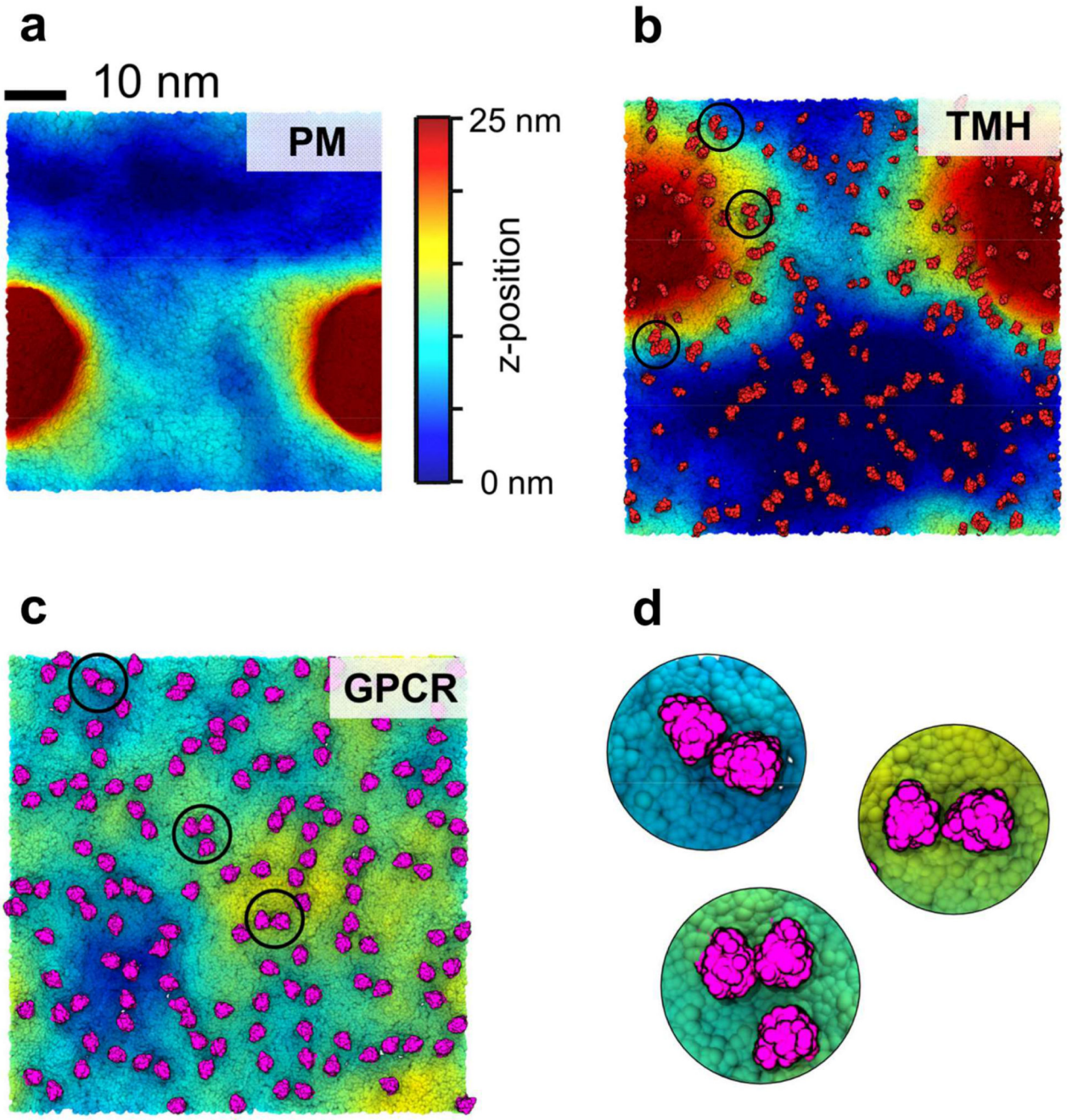

Figure 4. Membrane curvature and deformations.

Membrane curvature of the three simulation systems at 10 μs. The colour scale corresponds to the lipid headgroup z-position using a 0 (blue) to 25 nm (red) scale. (**a**) **PM** system without any proteins. (**b**) **TMH** system with the proteins shown in red. (**c**) **GPCR** system with the proteins shown in pink. (**d**) Zoom in on selected S1P1 oligomers within the **GPCR** system shown in (**c**).

Europe PMC Funders Author Manuscripts

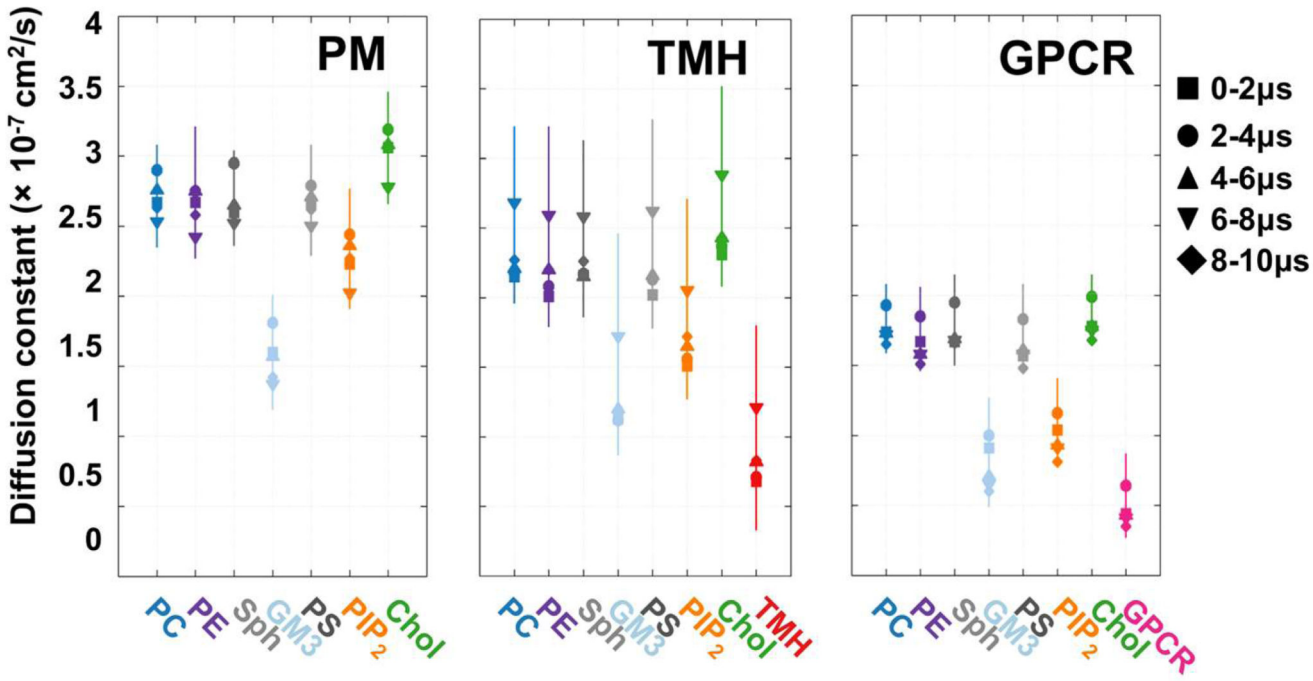

Figure 5. Lipid diffusion.

Lateral diffusion constant as obtained from fitting to the mean square displacement for each lipid species and the proteins within different intervals using a timestep of 5 ns for the **PM**, **THM** and **GPCR** systems.

Europe PMC Funders Author Manuscripts

Europe PMC Funders Author Manuscripts

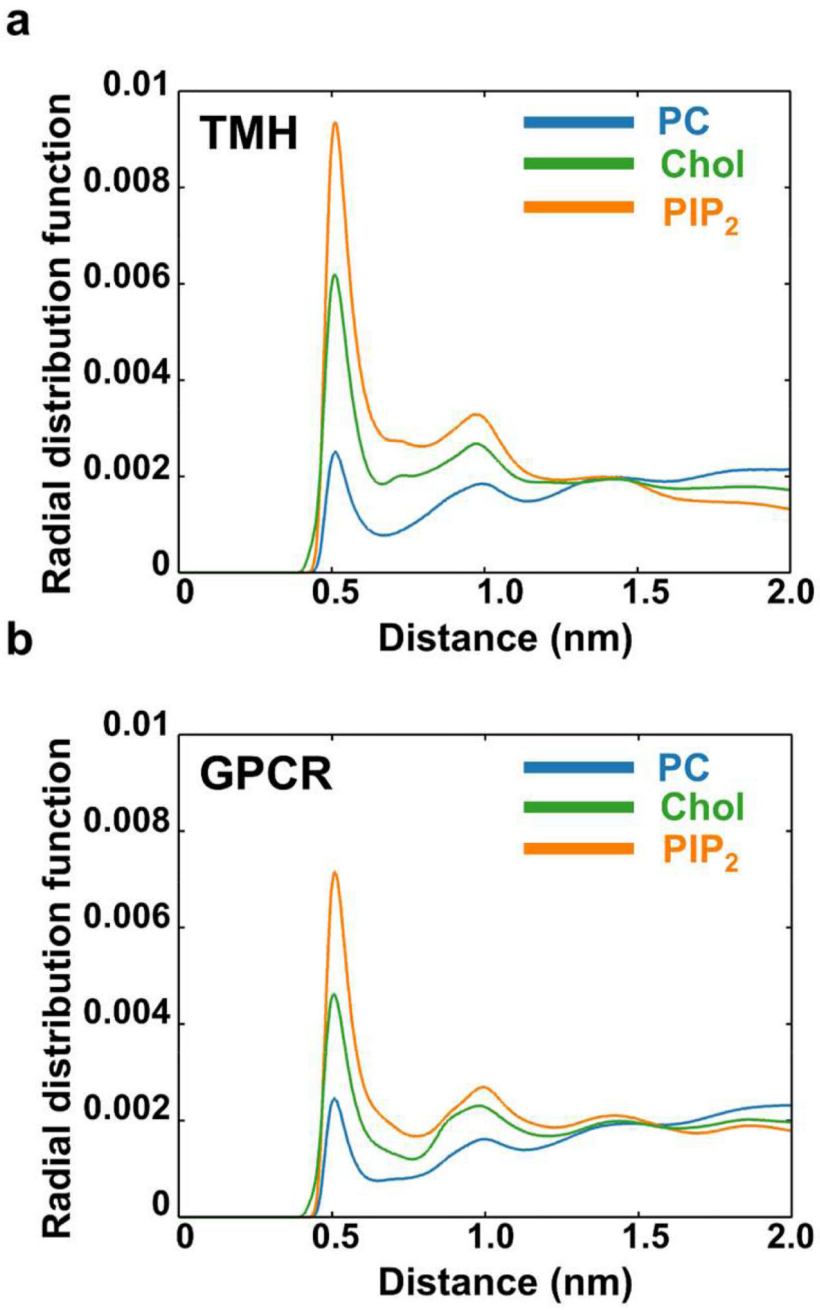

Figure 6. Protein-lipid interactions.

Protein-lipid interactions measured by the spherical radial distribution function of PC, Cholesterol and PIP_2 lipid species around the protein (blue = PC, green = cholesterol, orange = PIP_2). (**a**) **TMH** system. (**b**) **GPCR** system. The area under the curve of the radial distribution has been normalized to unity to allow for comparison between lipid species. Radial distribution functions for all lipid species are shown in SI figure S8.

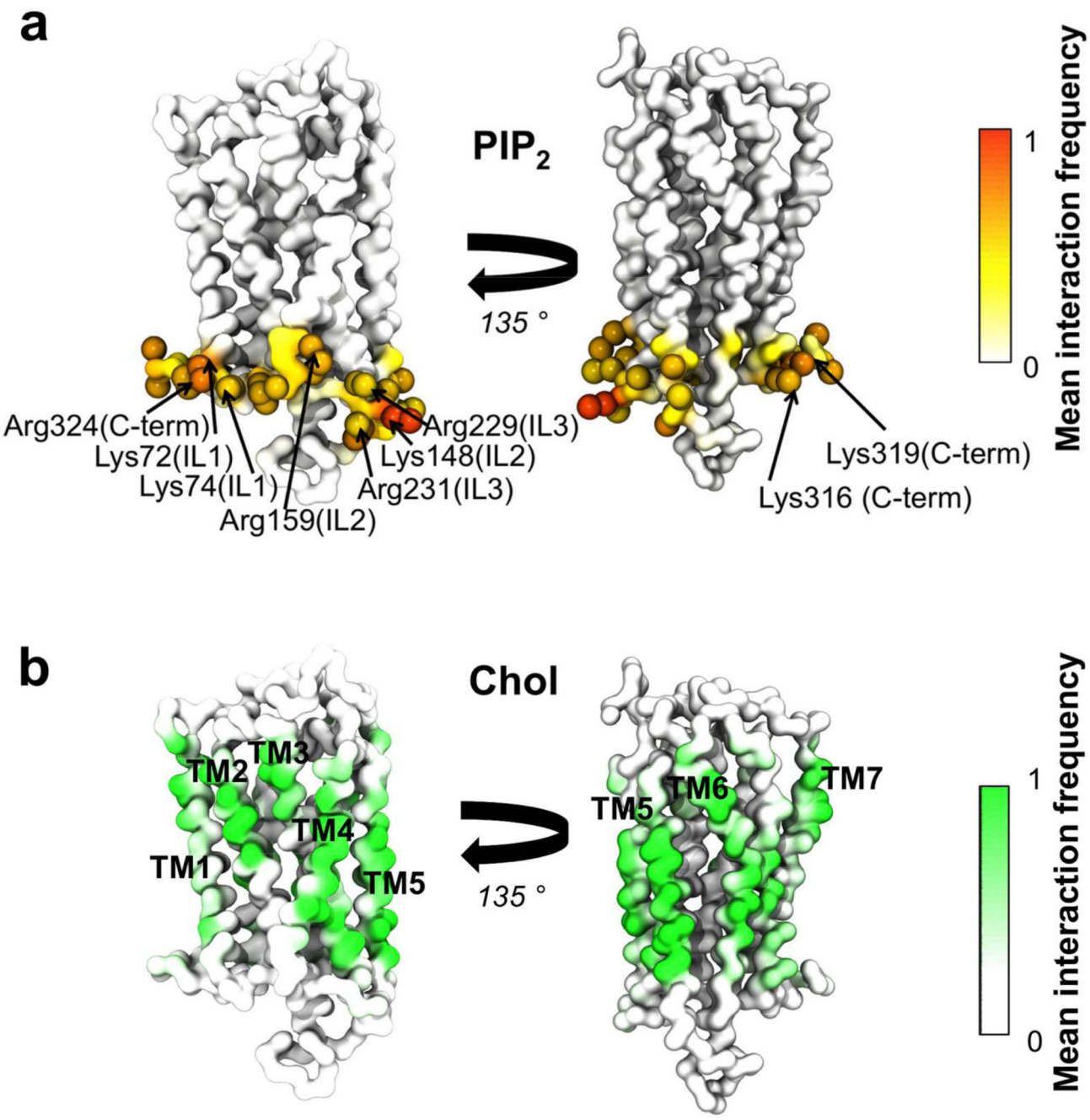

Figure 7. Protein-lipid interactions in the GPCR receptor system.

Interactions between PIP_2 and cholesterol have been mapped onto the structure of one of the S1P1 receptors. The colour scale illustrates the mean fraction of time there is an interactions with all 144 repeats of the S1P1 receptor. Thus, a value of 1 indicates a lipid forms a contact with a given residue in all proteins over the entire duration of the simulation. (**a**) Interactions between the phosphoryl head group of PIP_2 and the S1P1 receptor. Residues having interactions more than 75% of the time are shown as spheres. The basic residues within the

residues have been labelled. (**b**) Interactions between any part of the cholesterol molecule and the S1P1 receptor.

Europe PMC Funders Author Manuscripts

Europe PMC Funders Author Manuscripts

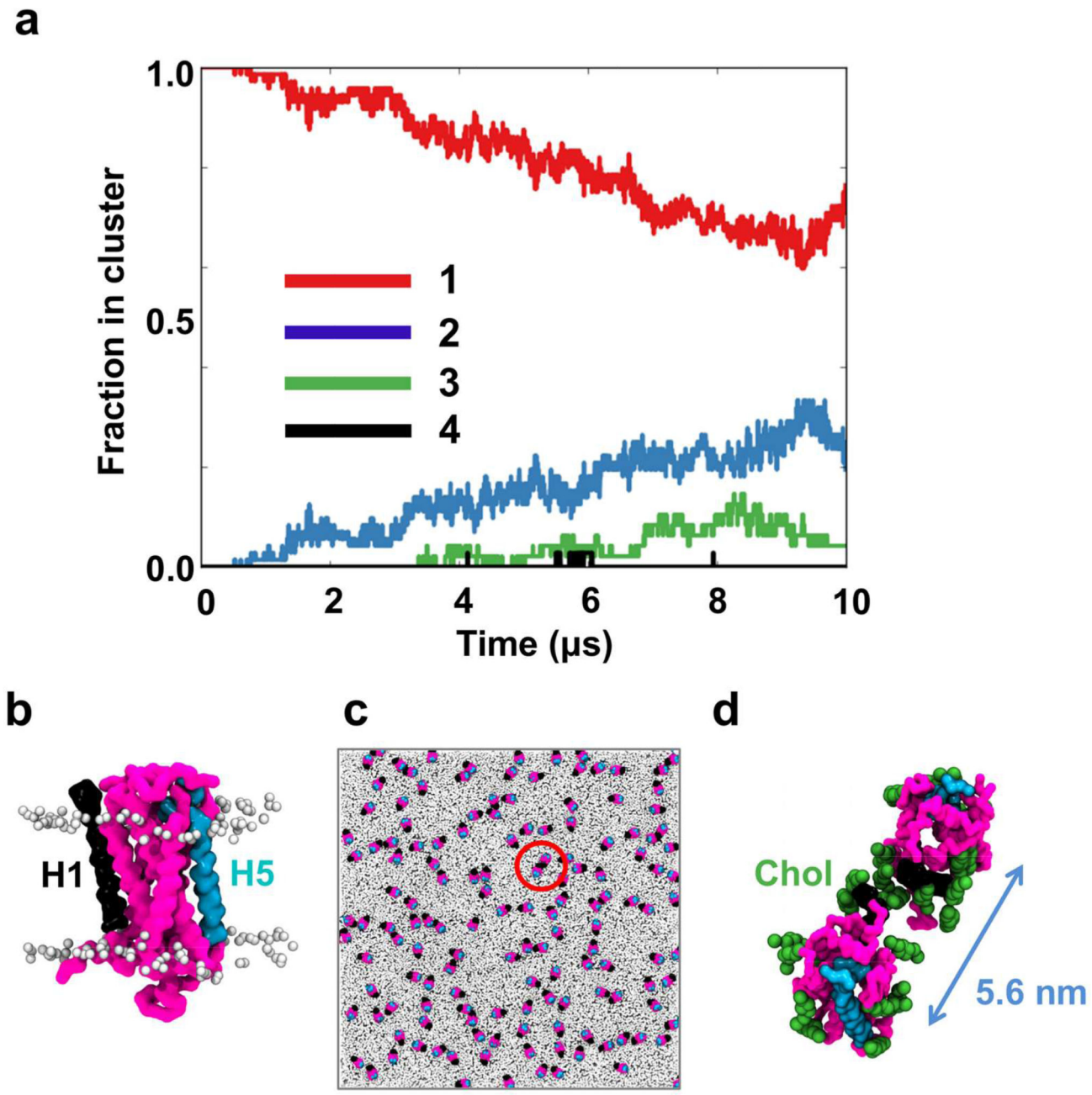

Figure 8. GPCR oligomerization.

(**a**) The clustering of S1P1 receptors within the **GPCR** system over time. Clustering was calculated using a cut-off distance of 6.0 nm between the centres of mass of adjacent proteins. (**b**) a S1P1 receptor (pink) with transmembrane helix 1 (H1; in black) and transmembrane helix 5 (H5; in cyan). (**c**) Orientation of the 144 GPCRs after 10 μs of simulation with the proteins colored as in (b) while all lipids are colored in light gray (**d**) zoom in on one of the GPCR oligomers. Cholesterol molecules within 5 Å of the proteins

are shown in green and the distance between the centres of mass of the two proteins is shown in blue.

Europe PMC Funders Author Manuscripts